ISSN 1063-7761, Journal of Experimental and Theoretical Physics, 2006, Vol. 103, No. 3, pp. 385–397. © Pleiades Publishing, Inc., 2006.

ORDER, DISORDER, AND PHASE TRANSITIONS IN CONDENSED SYSTEMS

Magnetic Characterization of a Hydrogen Phase Trapped Inside Deep Dislocation Cores in a Hydrogen-Cycled PdH_x ($x \approx 4.5 \times 10^{-4}$) Single Crystal¶

A. G. Lipson[a, b], B. J. Heuser[a], C. H. Castano[a], B. F. Lyakhov[b], and A. Yu. Tsivadze[b]

[a] *University of Illinois at Urbana-Champaign, Department of Nuclear, Plasma and Radiological Engineering, Urbana, IL, 61801, USA*

[b] *Institute of Physical Chemistry and Electrochemistry, Russian Academy of Sciences, Moscow, 119991 Russia*

e-mail: lipson@uiuc.edu

Received March 23, 2006

Abstract—The magnetic characterization of Pd single crystals deformed by cycling in a hydrogen atmosphere has been performed. Based on evidence obtained from thermal desorption analysis, it is shown that the condensed hydrogen phase formed inside deep dislocation cores in PdH_x (x = H/Pd $\approx 4.5 \times 10^{-4}$) is tightly bound with a Pd matrix. The activation energy of hydrogen desorption from these cores was found to be as high as e = 1.6 eV/H-atom, suggesting the occurrence of a strong band overlapping between Pd and H atoms. SQUID measurements carried out in a weak magnetic field ($H < 5.0$ Oe) showed an anomalous diamagnetic contribution to the DC and AC magnetic susceptibilities of the PdH_x sample at $T < 30$ K resulting in the presence of the hydrogen phase. It is suggested that the anomalous diamagnetic response in PdH_x is caused by the presence of a hydrogen dominant phase, tightly bound with a Pd matrix inside the dislocation cores (nanotubes).

PACS numbers: 74.78.Fk, 74.10.+v, 61.72.-y

DOI: 10.1134/S1063776106090081

1. INTRODUCTION

The study of the trapping and interaction of hydrogen atoms inside metallic nanostructures (dislocation cores and nanotubes) is important in order to increase the efficiency of hydrogen storage in metals (e.g., palladium) as well as to promote electron transport applications in nanotechnology [1, 2]. Recently, Ashcroft presented arguments that hydrogen-dominant metallic alloys, particularly, dense hydrides of the IVa group, might demonstrate high-temperature superconductivity (HTS) even in a modest external pressure range [3]. This argument is based on the similarity of the electronic structures of hydrogen-dominant metal alloys and of the superconductor MgB_2 [4]. According to Ashcroft's reasoning, HTS of highly loaded metal hydrides must be due to the overlapping of metal–hydrogen bands. The high electron concentration and optical phonon energy result in a strong electron–phonon coupling. The advantage of hydrogen-dominant hydrides for achieving HTS is that in a chemical sense, they have already undergone a sort of "precompression," and once impelled by external pressure they enter the metallic phase and the electrons from both the hydrogen and the metal may participate in common overlapping bands [3].

There is another approach to achieve a compressed, metal hydride state with a high coupling constant that may serve as a model alloy to search for HTS in hydrogen-dominant metallic systems. Heuser et al., using a small-angle neutron scattering (SANS), showed that dislocations created in Pd film hydrogen cycling are strong abundant traps of interstitial hydrogen [5, 6]. The concentration of hydrogen (x is an atomic ratio H/Pd) near the dislocation depends on the hydrogen distribution with respect to the distance from the core or on the hydrogen binding energy [5, 6]. After cycling of a Pd single crystal film with deuterium gas, a large number of dislocations ($N_d \geq 2 \times 10^{11}$ cm^{-2}) were generated [5]. Without annealing, the residual hydrogen left in the Pd sample ($x \approx 5.5 \times 10^{-3}$), which exists in an α-phase with a concentration of 4–5 deuterons per 1 Å of the dislocation line [6]. This level of residual hydrogen was associated with a low hydrogen binding energy of $\varepsilon_H = 0.2$ eV. However, a smaller amount of residual hydrogen atoms ($x \sim 10^{-4}$) was found to have a remarkably higher binding energy $\varepsilon_H \approx 0.7$ eV. In this case, most absorbed hydrogen atoms are tightly bound inside deep dislocation cores [7].

Recently, Maxelon et al. [8] found that the radius R_H of the residual hydrogen distribution with respect to dislocation core is strongly affected by the concentration of hydrogen atoms. They have shown that R_H is

¶ The text was submitted by the authors in English.

reduced from 13 to 4.9 Å with a decrease in x from 1×10^{-2} to 1.7×10^{-3}. At lower x, the minimal value of $R_H \approx b = 2.75$ Å (where b is the Burgers vector) might be anticipated.

The deep dislocation core filled with hydrogen atoms could be regarded as a sort of a nanotube with an effective diameter of about two Pd Burgers vectors [8]. Moreover, it is implied that within the deep dislocation core ($R_H < b$), the local hydrogen concentration might be large enough to provide the ability of overloading the Pd beyond $x = 1$ [9]. The pressure inside the cores of edge dislocation is comparable to a local palladium bulk modulus (up to 120 GPa [10]) and the conditions of both hydrogen precompression and external pressure impelling are fulfilled. This is the basis for the above statement that a compressed metallic hydride state or quasimetallic hydrogen phase [11–14] can be obtained via an alternative route, by trapping at dislocation cores in deformed Pd. The electron properties of saturated compressed Pd hydrides have not been studied previously because these compounds are unstable at ambient conditions [15, 16]. However, anomalies in the electron transport and magnetic properties in highly loaded Pd hydrides (including H-cycled Pd compounds) below 300 K have been reported [17–19].

At least above 3.0 mK, annealed Pd metals do not show superconductivity [15]. In contrast, Pd hydrides with a loading ratio $x > 0.8$ are superconductors with a relatively high T_c [20]. The importance of increasing the loading from $x = 0.81$ to $x = 1.0$ resulted in a dramatic growth of T_c in the Pd hydrides (from 1.5 to 8–9 K [21, 22]). Although the superconducting effects in Pd hydrides have not been fully explained yet, it is suggested that their superconductivity is based on strong electron–phonon coupling to the optical modes and requires suppression of the spin fluctuation in the Pd lattice and *sd* hybridization of hydrogen and Pd electrons [16].

If the state of the condensed hydrogen phase inside the dislocation cores were a hydrogen dominant metallic alloy, the diamagnetic behavior of this phase, although affected by the magnetic contribution of the palladium lattice and impurities, would be anticipated at a low temperature [11–13]. On the other hand, in the hydrogen-dominant Pd dislocation cores in Pd, the conditions required in [3] seems to be fulfilled: sufficient pressure, strong electron–phonon coupling, and high local optical mode energy. This suggests the occurrence of a superconducting transition above the critical temperature of the bulk PdH_x measured at ambient conditions [18, 19]. However, the observation of such a transition from a hydride phase inside the dislocations confined in the Pd matrix could be feasible when two referenced conditions on the dislocation network are satisfied: (1) there is a sufficiently large number of dislocations within the Pd crystal that contain tightly bound compressed hydrogen; (2) the network of dislocations is organized in the form of closed loops [23], which can carry a persistent current [24].

In this work, we studied the structural and magnetic properties of PdH_x with the very low average loading ratio $\langle x \rangle \approx 4.5 \times 10^{-4}$ that was produced by cycling the pure Pd single crystal in a H_2 atmosphere with final annealing at $t = 300$°C. Thermal desorption analysis (TDA) showed that the residual hydrogen precipitates as a condensed phase within the deep dislocation cores. Magnetic measurements recorded the appearance of a strong diamagnetic contribution of the net PdH_x–Pd phase in the Pd matrix at $T < 30$ K (in a weak magnetic field $H \leq 5.0$ Oe), and an antiferromagnetic behavior in the higher magnetic field. The thermal desorption analysis and magnetic measurements together suggest that the dislocation nanotubes in the hydrogen-cycled Pd sample contains a diamagnetic condensed hydrogen/Pd hydride phase at low temperatures.

2. EXPERIMENTAL

To exclude the effect of impurities on the magnetic properties of the PdH_x system, a 99.999% pure Pd single crystal produced by Metal Crystals and Oxides of Cambridge, UK was employed in this work. The cylindrical ingot was grown using the Czochralski method with the [110] axis, a length of 10 cm, and a diameter of about 1.0 cm. A sample with dimensions of $2.7 \times 2.7 \times 0.6$ mm^3 and a weight of 52 mg was cut from the as-grown ingot using a low-speed diamond saw, and mechanically polished to remove surface irregularities. Then, this single crystal was annealed in a high vacuum ($p = 10^{-8}$ Torr) at a temperature of 800°C for 5 h. The annealed pristine Pd single crystal served as a reference and is labeled the "Background" sample, or "bgr," and the appropriate TDA and magnetic measurements were conducted on this sample prior to the hydrogen cycling.

In order to create a condensed hydrogen phase in the Pd sample, a H_2 gas cycling procedure was applied. The sample was loaded and degassed twice. The pristine Pd (bgr) sample (after TDA and magnetic measurements) was loaded at a pressure of 930 Torr at temperature 390 K and degassed in a vacuum of 10^{-6} Torr at a temperature of about 400–430 K. After the cycling, the PdH_x sample was subjected to a final annealing at temperature 570 K and pressure 10^{-8} Torr for 2 h. This post-cycled PdH_x crystal is labeled "Foreground" sample, or "fg."

A high-vacuum thermal desorption technique was used to estimate the residual hydrogen concentration in the H_2-cycled Pd sample. The sample was heated within the 20–900°C temperature interval in the linear regime, at the rate of 9.0 K/min in a high-vacuum (10^{-8} Torr) chamber of a quadrupole mass spectrometer. After analyzing the desorption species (Fig. 1) and comparing the yield with the data from the Pd(bgr) (taking the residual hydrogen background in the vac-

uum chamber into account), we were able to calculate the real hydrogen desorption peak area and the temperature of its maximum. It was found that the background hydrogen desorption pressure (Pd(bgr) sample plus the residual hydrogen in the chamber) was at least five to ten times lower than the H_2 pressure caused by the PdH_x(fg) samples (Fig. 1, curves *1* and *2*).

For quantitative estimation of the final average loading ratios x = H/Pd, we conducted special calibration measurements with a known mass (0.3 mg) of TiH_2 powder that has a decomposition temperature near 400°C. Comparing the hydrogen pressure in the chamber obtained from the TiH_2 powder with the PdH_x, we obtained an estimation of the residual hydrogen content in the H_2-cycled Pd single crystal.

Magnetic measurements were carried out with a 1T-SQUID "Quantum Design MPMS-3" using DC-magnetization and AC-susceptibility modes. The Pd(bgr) and PdH_x(fg) samples were placed in a gelatin aligned in the direction to the pick-up coil and covered with a small piece of cotton. The initial magnetic moment of the capsule with a piece of cotton, in a low magnetic field $H < 10.0$ Oe was measured to be $M < 10^{-8}$ emu, well over the studied temperature interval (2.0–350 K).

Measurements with a calibration magnetic fluxgate showed that without the application of the special ultralow field condition, the SQUID has the residual magnetic field of $\Delta H \approx -0.2$ G. Ultra-low field installation with degaussing of the shielding produces an almost zero field (the remanent field is less than 1 mG). In the DC-magnetization mode, the SQUID was calibrated with a Pd standard. It was found that the sensitivity of the SQUID with the capsule and sample is higher than 5×10^{-8} emu. To measure the magnetic moment versus temperature in the zero-field cooling (ZFC) regime, the samples were cooled from $T = 298$ K to $T = 2.0$ K at $H = 0$ after installation of zero field at room temperature. The measurements of the $M(H)$ function at constant temperatures were carried out in the automatic regime. After the measurements of the $M(H)$ curves at given temperatures were completed, the sample was heated at $H = 0$ to $T = 350$ K. The cooling of the Pd samples to the next temperature was conducted at the nominal field $H = 0$ (without zero-field installation) after annealing of the capsule at 350 K for 10 min inside the SQUID.

The AC measurement of the real and imaginary parts of the susceptibility for the Pd samples was carried out at $H = 0$ with a driving amplitude of $h = 1.0$ Oe and a magnetic field frequency of $f = 20$ Hz. During this measurement, the samples were cooled to 2.0 K at $H = 0$ without a special zero-field installation. Before the AC measurement with the Pd(bgr) and PdH_x(fg) samples, the setup was calibrated in the range 2–10 K using pieces of high-purity Pb and Nb shaped similarly to the Pd samples.

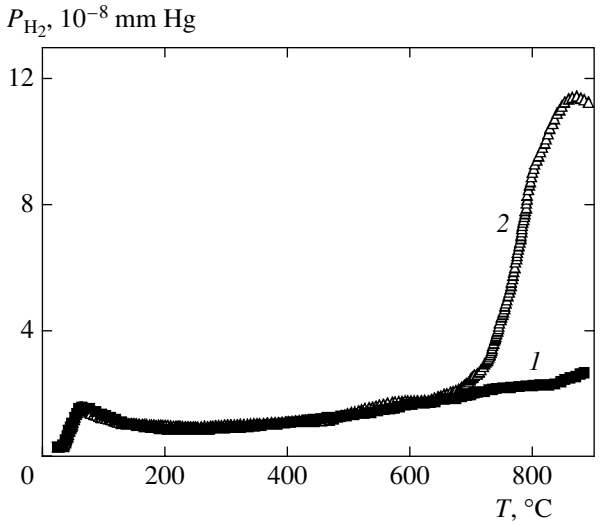

Fig. 1. Thermal desorption spectra for the Pd single crystal: curve *1* corresponds to Pd(bgr) before H_2 cycling and curve *2* to PdH_x(fg) after H_2 cycling.

3. EXPERIMENTAL RESULTS

3.1. Hydrogen Thermal Desorption Analysis

TDA performed with annealed Pd(bgr) samples in the temperature range 20–900°C showed a total absence of any hydrogen desorption peaks. The hydrogen pressure in the vacuum chamber throughout the studied temperature intervals did not exceed 2×10^{-8} Torr (Fig. 1, curve *1*). This H_2 pressure value equals the residual hydrogen background in the chamber. Therefore, the TDA with the annealed Pd single crystals indicates that there was no trapped hydrogen in the sample. Similar measurements performed for the PdH_x(fg) sample showed an H_2 pressure behavior at $T < 700$°C that was similar to the Pd(bgr) sample (Fig. 1, curve *2*). This observation proves that there is no hydrogen (in the α- or β-phase) in the regular lattice of the H_2-cycled PdH_x(fg) sample. But at $T > 700$°C, the hydrogen desorption (curve *2*) increased and the postcycled (fg) sample produced a pronounced peak with a maximum at 870°C. (We note that two curves shown in Fig. 1 terminate at 920°C. This is the upper limit of the TDA system.) The analysis showed that the H_2 pressure at 870°C is about six times higher than that observed at the same temperature range in the background measurements. Integration of the H_2 peak for PdH_x(fg) (with subtraction of the background) and comparison of its area with calibration data obtained for TiH_2 powder allowed the estimation of the effective loading ratio x = H/Pd averaged over the PdH_x(fg) sample volume, as $x = (4.5 \pm 0.5) \times 10^{-4}$. The averaged value of x is smaller than expected for any known stable phase of Pd hydride

[16]. Considering that after the H_2 cycling, the sample undergoes an additional annealing at 570 K, which causes the decomposition of the residual α-phase in the lattice [16], we assume that all remaining hydrogen detected in the cycled Pd single crystal is located in the dislocations but not in the regular lattice. Extrapolating the results of SANS measurements performed in [8] for various residual hydrogen concentrations in Pd polycrystals ($x \geq 1.7 \times 10^{-3}$), we estimate a radius RH of the residual hydrogen distribution with respect to dislocation cores. At $\langle x \rangle$ = H/Pd = 4.5×10^{-4}, the value $R_H \approx 2.8$ Å is close to the minimal radius of the hydrogen capture in Pd (the Burgers vector).

In order to estimate the binding energy of hydrogen within the Pd, the hydrogen activation energy was calculated. The formal kinetics Garlick–Gibson model may be used to estimate the kinetic parameters of the second-order thermal activation processes by accounting for the rising edge of the hydrogen release peak [25]:

$$\varepsilon_H = k_B \frac{T_2 T_1}{T_2 - T_1} \ln \frac{P_2}{P_1},$$

where k_B is the Boltzmann constant, and P_1, P_2, and T_1, T_2 are two hydrogen pressure and temperature points ($T_2 > T_1$ and $P_2 > P_1$). The result of this analysis is ε_H = 1.7 ± 0.2 eV. It reflects the effective binding energy of trapped hydrogen in the Pd lattice.

To verify this value of ε_H, another independent method was used to determine the activation energy. In contrast to the Garlick–Cibson model, this method includes the hydrogen diffusivity in Pd. Based on the solution of the hydrogen diffusion equation (with respect to the hydrogen flux $J_0(T)$ spilling out of the Pd into vacuum) in a Pd single crystal [26] with the boundary and initial conditions (hydrogen concentration before and after initial thermal desorption and peak temperature T_{max} of thermal desorption), $J_0(T)$ is finally obtained as [27]

$$J_0(T) = \frac{2\pi D_0 C_0}{L} \exp\left(-\frac{\varepsilon_H}{k_B T}\right) \times \sum_{n=1}^{\infty} n \frac{\int_0^L \sin(n\pi x/L)dx}{\int_0^L \sin^2(n\pi x/L)dx} \times \exp\left[\frac{aD_0\varepsilon_H n^2\pi^2}{k_B L^2} \int_{-\varepsilon_H/k_B T}^{\varepsilon_H/k_B T} \frac{e^{-w}}{w^2} dw\right], \quad (1)$$

where D_0 is the preexponential factor of hydrogen diffusion in Pd [16], C_0 is the initial concentration of hydrogen in the sample (from before, $x = 4.5 \times 10^{-4}$), L is the sample thickness (6×10^{-2} cm), N is the index of the eigenvalue of the separation constant in the solution of the diffusion equation, and a = 9.0 K/min is the heating rate at T_0 = 296 K. Evaluating the first five terms of function (1) with respect to the activation energy, we found that $\varepsilon_H = 1.6 \pm 0.3$ eV can be used to satisfactorily describe the experimental peak with T_{max} = 1143 K (870°C). This more accurate value of ε_H is very close to that obtained from the simple model [25].

The magnitude of the activation energy of hydrogen desorption that was found for the PdH_x(fg) crystal is well above the H-trapping activation energy derived for H_2-cycled polycrystalline cold-worked Pd that has an extremely low bulk hydrogen concentration captured inside the deep dislocation cores ($\varepsilon_H \approx 0.7$ eV) [6, 7]. This provides us with a strong argument that the hydrogen is bound solely inside the deep core sites. Thus, the TDA results show that the hydrogen atoms are tightly bound inside the deepest dislocation cores and can be fully removed only at very high temperatures ($T \geq$ 1000°C), which would suggest a full recrystallization of the Pd sample. The TDA results allow us to conclude that PdH_x samples that are produced by H_2 gas cycling of the Pd single crystals followed by annealing at T = 570 K contain no hydrogen atoms in their crystalline lattice except those that are tightly bound inside the deepest dislocation cores (or "dislocation nanotubes") of the minimal radius ε_H = 2.75 Å.

3.2. Magnetic Measurements

The DC-mode ZFC experiment showed that in a weak magnetic field (H = 0.5 Oe), the magnetic moment M of H_2-cycled PdH_x(fg) samples in the temperature range $2 \leq T < 50$ K is significantly lower than $M(T)$ for the original Pd(bgr) single crystals (Fig. 2a). The difference between the moments of the cycled sample and the original single crystal, $\Delta M = M(PdH_x) - M(Pd)$ reflects the contribution of the condensed hydrogen phase inside the deep dislocation cores. This net difference tends to increase at $T \leq 30$ K. There was no temperature dependence observed for ΔM in the field-cooling (FC) measurements at high magnetic fields (H = 1000 Oe), Fig. 2b. The moment of the PdH_x is about 4–5% lower than that of the Pd(bgr) and a nearly constant negative net difference ΔM is detected within temperature range 2–298 K.

The AC measurements showed that the real (in-phase) part χ' of the magnetic susceptibility at $H = 0$ for the PdH_x(fg) sample tended to decrease compared to that of the Pd(bgr) single crystal below 130 K; at a lower temperature $T \approx 20$ K, it becomes several times less than χ' for Pd(bgr), Fig. 3a. Therefore, the PdH_x–Pd contribution in $\chi'(T)$ was found to be strongly negative at $T \leq 18$ K (Fig. 3c), which was similar to the $\Delta M(T)$ behavior in the DC measurements (Fig. 2a, curve *3*). The imaginary (out-phase) part χ'' of the mag-

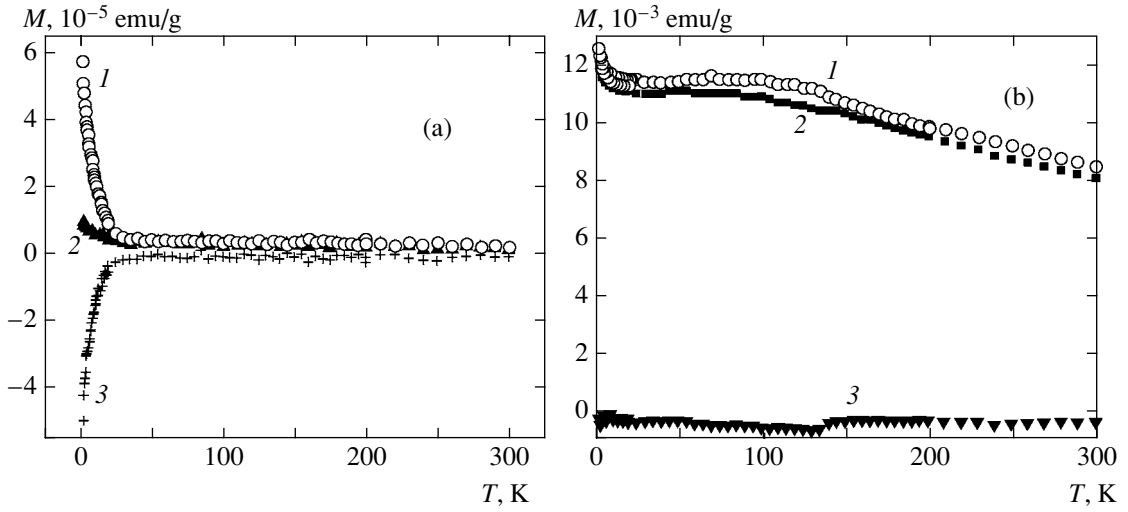

Fig. 2. DC magnetization versus temperature at (a) $H = 0.5$ Oe in the ZFC regime and (b) $H = 1000$ Oe in the FC regime: curves *1* correspond to Pd(bgr); curves *2* to PdH_x(fg); and curves *3* are the net subtraction $\Delta M = M(PdH_x) - M(Pd)$.

netic susceptibility for both the Pd(bgr) and PdH_x(fg) samples showed some transition corresponding to the dissipation process below 60 K (Fig. 4b). A broad maximum corresponding to the phase transition near 50 K was observed systematically in the earlier DC measurements with both bulk Pd and Pd-hydride samples [28,29]. For the H_2-cycled PdH_x(fg) sample, however, the magnitude of the electromagnetic energy dissipation is three times less than that of the original Pd(bgr). This significant reduction in χ'' could possibly indicate either an increase in conductivity or the reduction of the eddy current in PdH_x(fg) compared to that of the pristine Pd sample.

The measurements of the remanent magnetization M_r versus temperature at $H = 0$ were carried out after FC from $T = 300$ K to $T = 2.0$ K in the constant magnetic field $H = 1000$ Oe (Fig. 4). Both the PdH_x(fg) and Pd(bgr) samples showed a nonzero remanent magnetization within the 2–300 K temperature interval. It was found that the M_r value for PdH_x at low temperature is significantly larger than that for the Pd sample and tended to increase as the temperature decreased to 2.0 K. At higher temperatures, the remanent magnetization for PdH_x is lower than that for the pristine Pd(bgr). We note that the net $\Delta M_r = M_r(PdH_x) - M_r(Pd)$ moment behavior versus temperature is similar to $\Delta M(T)$ at $H = 0.5$ Oe, except being opposite in sign (curves *3* in Figs. 2a and 4). Both curves have a dramatic inflection near $T = 30$ K, in the positive direction for $\Delta M_r(T)$ and in the negative one for $\Delta M(T)$ at $H = 0.5$ Oe.

Therefore, we suggest the reduction in paramagnetic behavior is due to the appearance of the diamagnetic response in the condensed hydrogen phase bound inside the dislocation cores. To ascertain the origins of the dramatic decrease in the paramagnetic properties of PdH_x compared to the Pd single crystal at $T < 30$ K, we studied the magnetization of the PdH_x(fg) and Pd(bg) samples as a function of the applied magnetic field. These measurements were performed at constant temperatures of $T = 2$, 10, 50, 100, and 298 K in magnetic fields ranging from 0 to ±200 Oe. The $M(H)$ curves at $T = 2.0$ K for the Pd(bgr) and PdH_x(fg) samples that are presented in Fig. 5 have an essentially different character, especially below $H \approx 10$ Oe.

(1) The total width of the hysteresis loop at $M = 0$ for the PdH_x(fg) sample ($\Delta H = 7.45$ Oe) is much higher than that of the Pd(bgr) single crystal ($\Delta H = 3.7$ Oe).

(2) The slope of the magnetization (virgin) part of the hysteresis loop in the range $0 < H < 200$ Oe for the PdH_x(fg) sample is lower than that for Pd(bgr).

(3) Only the virgin part of $M(H)$ in the PdH_x(fg) sample has a point of inflection at $H \approx 3.5$ Oe, whose presence cannot be discerned from the pristine Pd(bgr) single crystal in the range 0–10 Oe.

The last observation could indicate a nonparamagnetic behavior of magnetization in H_2-cycled PdH_x. To verify this assumption, we tried to fit the experimental data for the Pd(bgr) and the PdH_x(fg) samples at $T = 2$ K below $H = 30$ Oe to the paramagnetic Langevin function,

$$M = M_0\left[\coth\left(\frac{\mu H}{k_B T}\right) - \frac{k_B T}{\mu H}\right],$$

where μ is the effective magnetic moment of Pd in the Bohr magnetons μ_B. We found that none of the M-functions fits the magnetization of PdH_x(fg) successfully and could describe the magnetization curve behavior at $H < 10$ Oe (the divergence is especially large below the inflection point at $H = 3.5$ Oe) [18]. In contrast, the magnetization of the pristine Pd(bgr) crystal could be satisfactorily fitted to the Langevin function, assum-

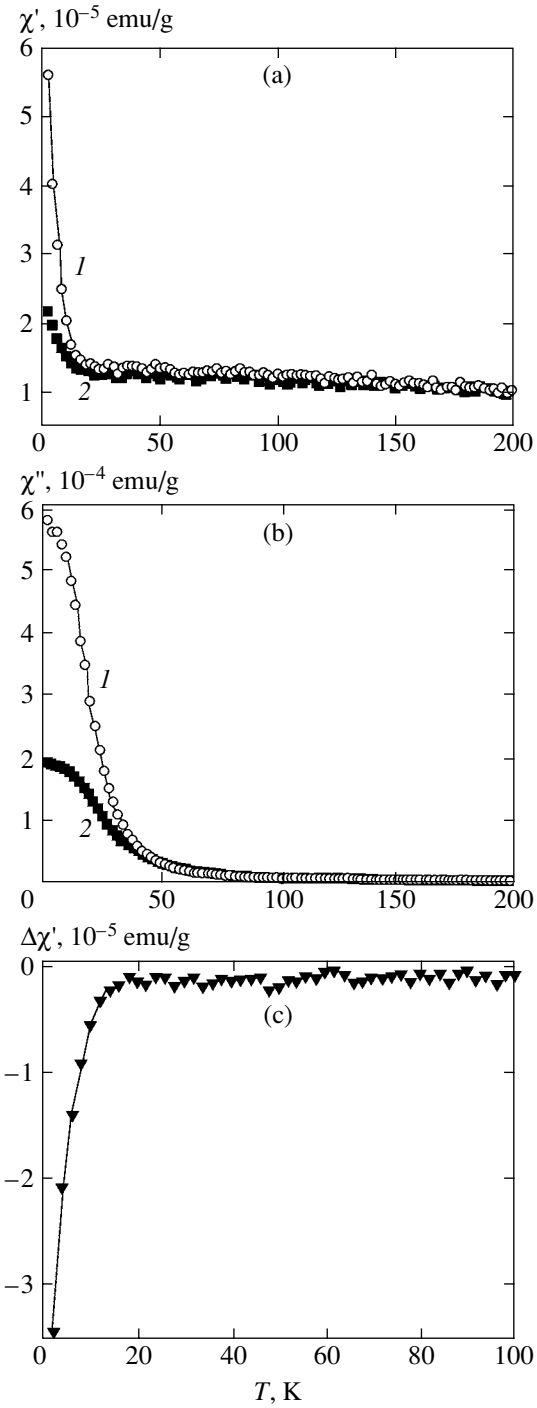

Fig. 3. AC susceptibility measurement after the sample cooling in a nominal zero field, i.e., without a zero-field installation: (a) real susceptibility $\chi'(T)$; (b) imaginary susceptibility $\chi''(T)$; and (c) net real susceptibility $\Delta\chi'(T) = \chi'(PdH_x) - \chi'(Pd)$. Curves *1* and *2* are for Pd(bgr) and PdH_x(fg), respectively.

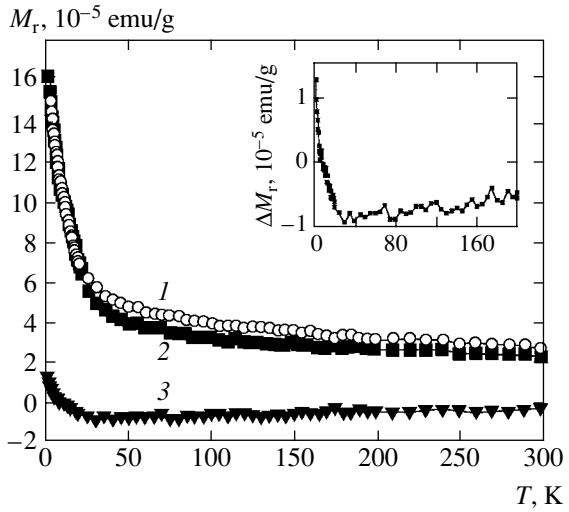

Fig. 4. Remanent magnetization as a function of temperature at $H = 0$ (after FC at $H = 1000$ Oe from 300 to 2 K): curve *1* is for Pd(bgr); curve *2* is for PdH_x(fg), and curve *3* is the net subtraction $\Delta M_r(T) = M_r(PdH_x) - M_r(Pd)$. The last one is shown in the inset in the enlarged scale.

ing that the effective magnetic moment of Pd is $\mu_B = 0.27\mu_B$ [18].

The dramatic contrast between the pristine Pd single-crystal and hydrogen-cycled Pd magnetization behavior is caused by the magnetization contribution of the PdH_x–Pd phase. The resulting net $\Delta M(H)$ function is obtained by subtracting the $M(H)$ data for Pd(bgr) from the $M(H)$ data for PdH_x(fg) and shows a minor hysteresis loop with a strong diamagnetic slope that is limited by the field values $H = \pm 20.0$ Oe (Fig. 5b). This "minor" loop with a high negative slope is located on the major loop with a much lower slope that expands over the higher magnetic field (by $H = \pm 200$ Oe).

Similar $M(H)$ dependences are obtained for Pd(bgr), PdH_x(fg), and the net PdH_x–Pd phase at $T = 10$ K (Fig. 6). The width of the hysteresis loop for the PdH_x(fg) sample is greater than that for the Pd(bgr), but the inflection in the virgin part of the $M(H)$ loop at $H <$ 5.0 Oe in PdH_x(fg) is less pronounced than at $T = 2.0$ K. The net $\Delta M(H)$ function at $T = 10$ K is quite similar to that at $T = 2$ K, but has a lower diamagnetic slope. At $T = 50$ K, the width of the hysteresis loop for PdH_x(fg) becomes closer to that of Pd(bgr), and the inflection in the virgin part of the PdH_x loop almost disappears (Fig. 7a). The changes of the hysteresis loop at $T =$ 50 K are accompanied by a dramatic decrease in the diamagnetic slope for the net $\Delta M(H)$ function. A minor diamagnetic loop at low H almost disappears, and the slopes at "low" ($H < 5.0$ Oe) and "high" ($10 < H <$ 200 Oe) magnetic fields become the same (Fig. 7b).

The widths of DC magnetization loops (coercive field) versus T for both the PdH_x(fg) and Pd(bgr) samples are presented in Fig. 8. In the sample with the condensed hydrogen inside the dislocation cores, the total width of the hysteresis loop tends to increase with decreasing temperature below 100 K. In contrast, for the pristine Pd(bgr) single crystal, the loop width is dra-

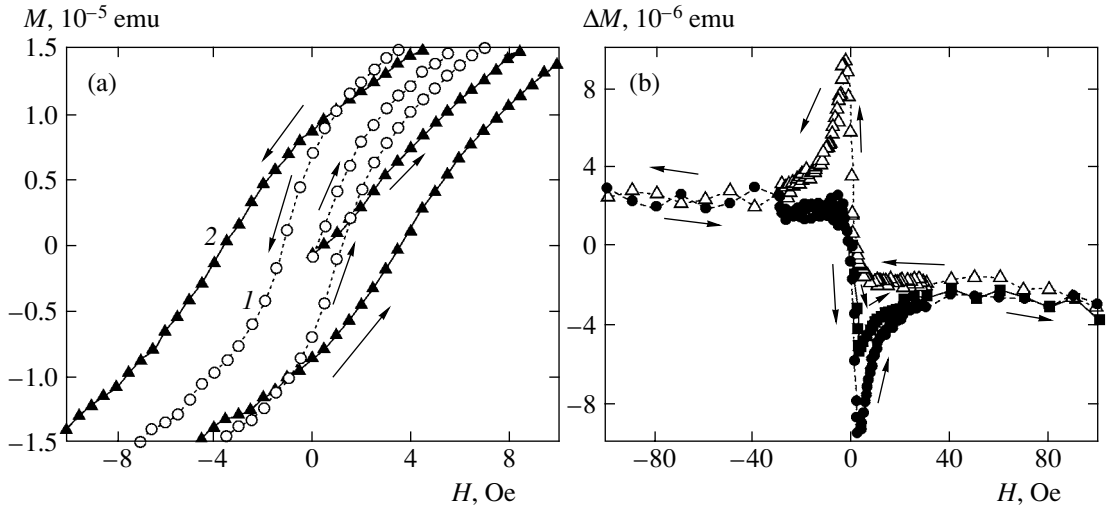

Fig. 5. (a) DC magnetization versus magnetic field $-200 \le H \le 200$ Oe at $T = 2$ K: curves *1* (circles) and *2* (triangles) are for Pd(bgr) and PdH_x(fg), respectively. The low-field part ($-10 < H < 10$ Oe) of the hysteresis loops is only shown. The arrows show the direction of the magnetic field change. (b) Net DC magnetization versus magnetic field for the PdH_x–Pd phase in "virgin"/magnetization curve (0 ⟶ 200 Oe, squares), demagnetization curve (200 Oe ⟶ –200 Oe, triangles), and remagnetization curve (–200 Oe ⟶ 200 Oe, circles). The lines are visual guides to the eye.

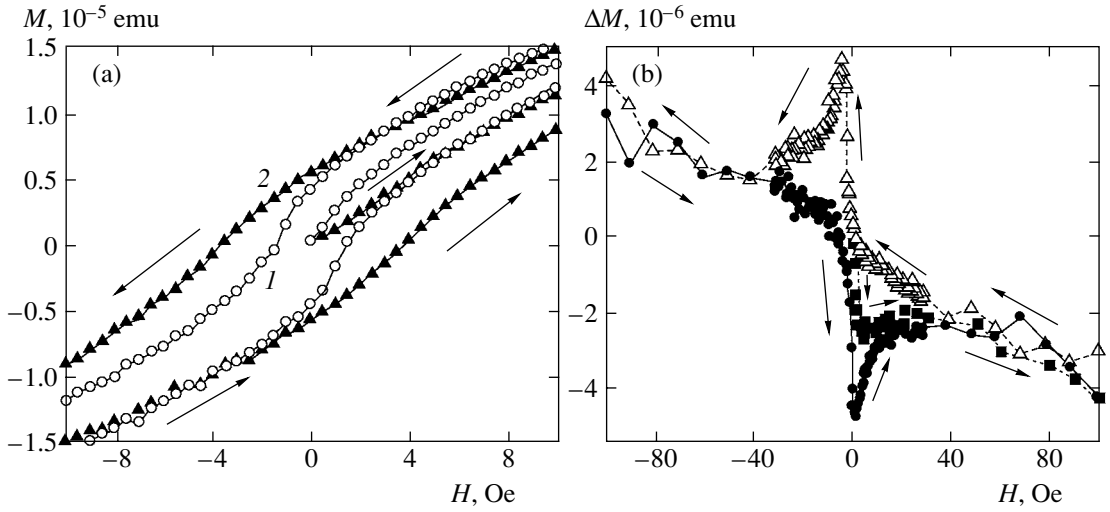

Fig. 6. The same as in Fig. 5 at $T = 10$ K.

matically reduced below 100 K. The differing behavior of the coercive field at $T < 100$ K for the PdH_x(fg) and Pd(bgr) samples suggests a difference in their magnetization versus H and indicates the contribution of the dislocations to the full magnetic moment of the PdH_x(fg) sample associated with the magnetic flux pinning.

The results of the $M(H)$ measurements allowed us to calculate the net slope susceptibilities $\chi = d(\Delta M)/dH$ for the PdH_x–Pd phase versus temperature (Fig. 9) for two different ranges of magnetic field: $0 \le H \le 5$ Oe (low magnetic field) and $5 < H \le 200$ Oe (high magnetic field). As seen from Fig. 9, in a low magnetic field, the slope susceptibility χ shows a strong diamagnetic transition at $T < 50$ K. In the high magnetic field, the clearly expressed dependence of $\chi(T)$ is not observed within the temperature interval 2–298 K. We note that the $\chi(T)$ dependences in the low and high magnetic fields are quite similar to each other above $T = 50$ K and demonstrate a significant divergence only at $T < 50$ K.

For comparison, curve *3* in Fig. 9 shows a net difference between the DC susceptibilities of Pd colloid particles (15 nm in diameter) and bulk Pd single crystal, based on the $\chi(T)$ data in [30]. It was established that the Pd particle size reduction is caused by the decrease in the paramagnetism of the Pd sample due to a Stoner-factor decrease caused by the distortion and partial disordering of the Pd lattice [29]. As seen from curve *3*, the

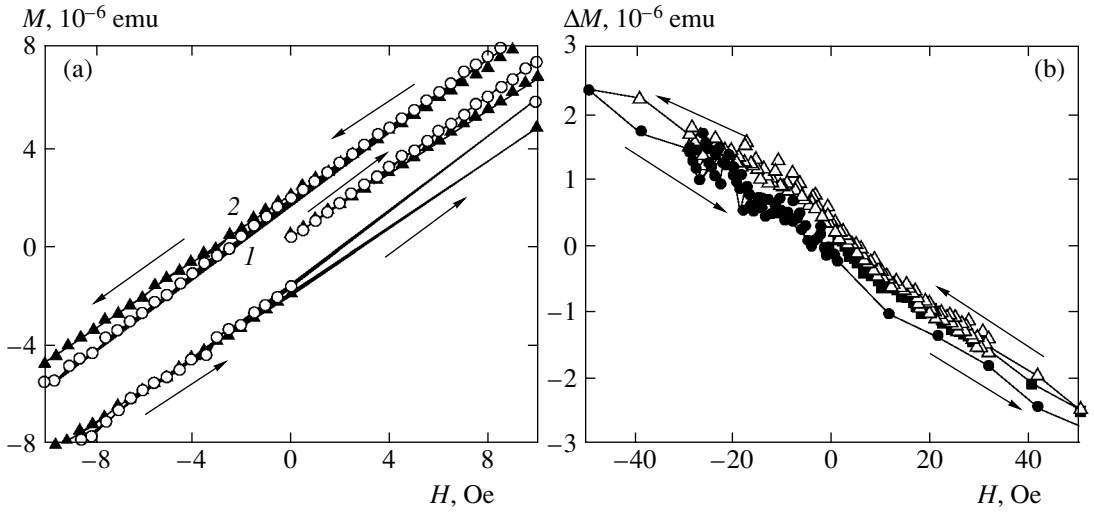

Fig. 7. The same as in Fig. 5 at $T = 50$ K.

$\chi(T)$ dependence for Pd nanoparticles with a bulk Pd subtraction is very similar to that for the PdH_x–Pd phase in a high magnetic field (Fig. 9, curve *2*). These two curves are both almost temperature-independent and show negative susceptibility. The distinction between these curves is only in an absolute value of χ, which is caused by the different size of the Pd particles involved in the $\chi(T)$ subtraction procedure (curves *2* and *3*).

To obtain a rough estimate of the particle (subgrain) size after H_2-cycling in the PdH_x(fg) sample, we consider the extrapolation of magnetic susceptibilities for both Pd(bgr) and PdH_x(fg) samples to $T = 0$ [30, 31]. Figure 10 shows a linear extrapolation of the initial trend of real AC susceptibility data (see Fig. 3a) for Pd(bgr) and PdH_x(fg) in the temperature range 30–200 K. We found that

$$\frac{\chi(T=0)}{\chi_0(\text{bulk})} = \frac{\chi'(PdH_x)}{\chi'(Pd)} = \frac{1.30\times10^{-5}\ \text{emu/g}}{1.43\times10^{-5}\ \text{emu/g}} \approx 0.91,$$

where χ' values for Pd(bgr) and PdH_x(fg) at $T = 0$ are regarded as bulk Pd and dispersed Pd, respectively. Extrapolating this data (plotted in [30, Fig. 4]) to a

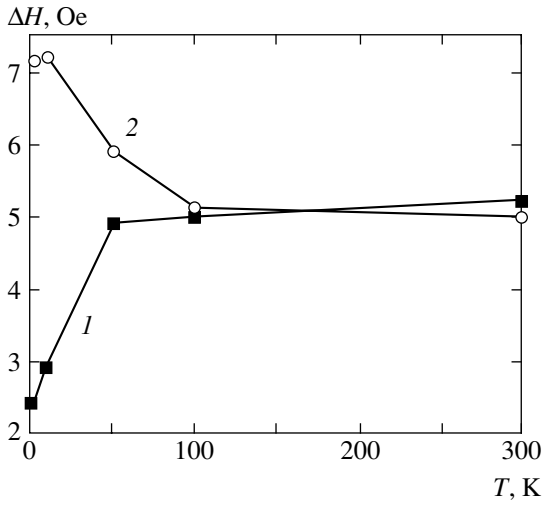

Fig. 8. The total width of the $M(H)$ hysteresis loops at $M = 0$ (coercive field) versus temperature: curves *1* and *2* are for Pd(bgr) and PdH_x(fg), respectively.

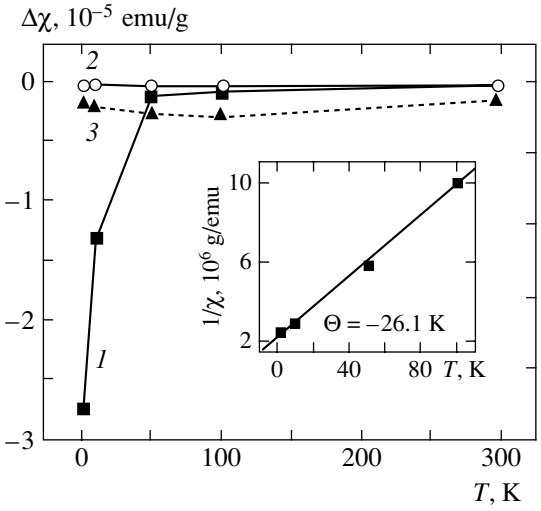

Fig. 9. The PdH_x–Pd phase net slope magnetic susceptibilities ($\chi = d(\Delta M)/dH$) versus temperature, calculated from the slopes of magnetization curves $M(H)$ for the low ($0 \le H \le 5$ Oe, curve *1*) and high ($5 < H \le 200$ Oe, curve *2*) ranges of the magnetic field. For comparison, curve *3* shows the $\Delta\chi(T)$ difference between the DC susceptibilities of colloid Pd particles 15 nm in diameter and bulk Pd (data taken from Fig. 1 of [30]). The solid lines are visual guides. The Curie–Weiss dependence of the high-field reciprocal slope susceptibility $1/(\chi - \chi_0)$ for the PdH_x–Pd phase at $T \le 100$ K ($\chi_0 = -1.0\times10^{-6}$ emu/g) is shown in the inset.

larger particle size R, we have found that $R \approx 60$ nm corresponds to the ratio $\chi(T = 0)/\chi_0(\text{bulk}) = 0.91$. This result suggests that during the hydrogen cycling, the sample "dispersed" into discrete subgrains, whose average diameter is found to be $d_s \approx 120$ nm. In the present case, this internal dispersity corresponds to the average dislocation spacing in a cycled single crystal given by $R_s \sim M/\sqrt{N_d}$, where N_d is the dislocation density [32–34]. The dispersion length is therefore associated with the dislocation density $N_d \approx 2.5 \times 10^{11}$ cm^{-2}, in good agreement with the SANS measurements discussed in the Introduction.

Hence, the weak diamagnetic response from the PdH_x–Pd phase in a high magnetic field over the temperature range 2–298 K (Fig. 9, curve *2*) could be ascribed to the internal dispersion of the Pd single crystal during its hydrogen cycling. The cycling generates a large number of dislocation loops, which results in the reduction of the block size of the original single crystal. This fact, however, cannot explain the $\chi(T)$ behavior of the PdH_x–Pd phase (Fig. 9, curve *1*) in a low magnetic field.

Conversely, we could suppose that the shape of the hysteresis loop for the PdH_x, including the inflection zone in the low field H (between 3 and 5 Oe) in the virgin part of the loop and the higher coercive field for the Pd(bgr) sample, is an effect of a frustrated spin-glass behavior in the PdH_x(fg) samples. This effect would then originate from the redistribution and aggregation of the rare ferromagnetic impurities in the Pd lattice by the hydrogen cycling. In this case, the ferromagnetic impurities would be localized in sites with a large internal strain, which are in the dislocations and saturate the PdH_x–Pd phase. According to this assumption, the PdH_x–Pd phase must demonstrate ferromagnetic behavior, obeying the Curie–Weiss law

$$\chi = \chi_0 + \frac{C}{T - \Theta},$$

where $\Theta > 0$ for ferromagnets or spin glasses. In the inset to Fig. 9, the Curie–Weiss dependence is presented as a function $1/[\chi(T) - \chi_0]$, constructed in accordance with the magnetic susceptibility points $\chi(T)$ for the PdH_x–Pd phase in a high magnetic field (Fig. 9, curve 2). The mean value of χ_0 is assumed to be roughly equal to $\chi(298\ \text{K}) = -1.0 \times 10^{-6}$ emu/g, suggesting a negative contribution due to the Stoner's decrease in paramagnetism. As can be seen, the $\chi^{-1}(T)$ curve in the temperature range $2 < T < 100$ K demonstrates a considerably negative Θ value ($\Theta = -26$ K), indicating the antiferromagnetic character of the PdH_x–Pd phase at low temperature.

This fact confirms that the Pd single crystal with a Fe concentration less or equal to 10 ppm did not contain sufficient ferromagnetic impurities to promote the ferromagnetic ordering of the dislocations at low temperatures. Furthermore, the paramagnetic reduction in the PdH_x sample compared to the original Pd indicates a corresponding Stoner-factor reduction in the PdH_x system due to the internal "dispersion" of the single crystal that accompanied the hydrogen cycling. Because a Stoner-factor reduction reflects a decrease in the exchange interaction between the electrons in PdH_x(fg) compared to Pd(bgr) [30, 31], we cannot expect the appearance of ferromagnetic behavior (caused also by the exchange interaction enhancement) in the hydrogen-cycled sample PdH_x.

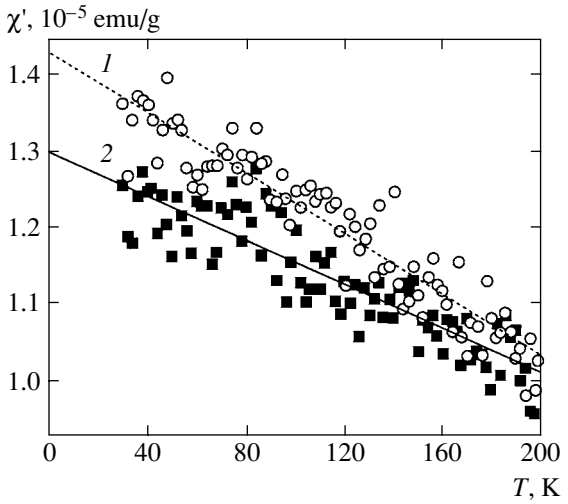

Fig. 10. Linear extrapolation of the real susceptibility $\chi'(T)$ in Fig. 3a to $T = 0$ in the range 30–200 K: curves *1* and *2* are for Pd(bgr) and PdH_x(fg), respectively.

4. DISCUSSIONS AND CONCLUSIONS

We consider the possible physical reasons for the anomalous diamagnetic response observed for the condensed hydrogen phase inside the deep dislocation cores PdH_x–Pd at $T < 30$ K in a weak magnetic field $H <$ 5 Oe. Analysis of the data that was obtained by the magnetic measurements both before the H_2-cycling (Pd(bgr)) and after cycling (PdH_x(fg)) allowed us to exclude the trivial reasons for this effect.

(1) The diamagnetic response that resulted from the net PdH_x–Pd phase at low temperature cannot be explained by the effect of segregation of the diamagnetic impurities in Pd, including residual hydrogen in the PdH_x ($x \approx 4 \times 10^{-4}$) sample, because the resulting diamagnetic response (the low-field diamagnetic slope at $T = 2$ and 10 K (Figs. 5b and 6b)) is several orders of magnitude above the total sum of the diamagnetic susceptibilities of these impurities.

(2) The simple reduction of paramagnetism in the PdH_x sample compared to the pristine Pd single crystal also cannot explain the behavior of $\chi(T, H)$ function for the PdH_x–Pd phase at $T < 50$ K and $H < 5$ Oe. The value

$\Delta\chi_{st} = \chi(\text{Pd colloid}) - \chi(\text{Pd bulk})$ is independent of temperature and magnetic field (Fig. 9, curve *3*) in accordance with the data in [30].

(3) The low-temperature and low-field behavior and inflection in the virgin part of the $M(H)$ hysteresis loop for PdH_x at $H \le 5$ Oe (at least at $T = 2$ and 10 K) cannot be described by the paramagnetic Langevin function, in contrast to the pristine Pd single crystal. Thus, the net loop of $\Delta M(H)$ referenced to the PdH_x–Pd phase would not be only a result of the subtraction of two paramagnetic functions with lower (PdH_x) and higher (Pd) moments (Figs. 5b and 6b).

(4) The full width of the hysteresis loop of $M(H)$ or the coercive field value for the PdH_x(fg) sample is much higher than that for the Pd(bgr) and shows a nonlinear increase below 100 K. In contrast, the coercive field for the Pd(bgr) sample decreases in the same temperature range (Fig. 8). We note that in Fig. 5a, the demagnetization (DM) and remagnetization (RM) curves for the PdH_x (fg) sample are not parallel one to another, as those curves for the Pd(bgr) sample. There is an anomalous diamagnetic contribution in both DM and RM curves corresponding to the low-field inflection zone in the magnetization curve at $T = 2$ and 10 K for PdH_x(fg). As a result, the DM and RM parts of the hysteresis loop near $M = 0$ exhibit a lower paramagnetic slope than that obtained for the Pd(bgr), giving rise to a broadening of the hysteresis loop at a lower field in PdH_x(fg) (Figs. 5a and 6a).

(5) Finally, the behavior of the magnetization (virgin) part of the $M(H)$ curve in PdH_x cannot be ascribed to the regrouping of the ferromagnetic impurities in the sample clue to hydrogen cycling, because the PdH_x–Pd contribution demonstrates antiferromagnetic behavior at $T \le 100$ K, at least where $H > 5$ Oe (Fig. 9, inset). On the other hand, the effects of the PdH_x irreversible magnetization below 100 K cannot, in principle, rule out the occurrence of a spin-glass behavior (coexisting with antiferromagnetism), reflecting the frustrated nature of Pd/PdH_x nanoparticles as localized spins [35].

To obtain a qualitative explanation for the anomalous diamagnetic response from the PdH_x–Pd phase in a low field, we suggest that in the PdH_x(fg) sample at low T, a strictly diamagnetic phase is present, which is caused by hydrogen precipitated inside dislocation cores. This response disappears in a high magnetic field, such as $H > 5.0$ Oe, or at higher temperatures $T \ge 50$ K. With this assumption, the full magnetic susceptibilities of the same Pd sample before (χ_{bgr}) and after (χ_{fg}) the H_2 cycling would be written as

$$\begin{aligned} \chi_{bgr} &= \chi_{Pd}(T) + \chi_i(T, H), \\ \chi_{fg} &= \chi_{Pd}(T) + \chi_i'(T, H) + (-\chi_{St}) \\ &\quad + [-\chi_{dH}(T, H)], \end{aligned} \tag{2}$$

where χ_{Pd} is the temperature-dependent lattice susceptibility of the Pd atoms, χ_i and χ_i' are, in general, the sum of the temperature- and field-dependent susceptibilities induced by para- and ferromagnetic impurities and their interaction with Pd before and after cycling, respectively, and $(-\chi_{St})$ is the Stoner-like reduction of Pd-lattice paramagnetism as a result of H_2 cycling. This cycling generates mechanical stress, causing "internal dispersion" of the original Pd single crystal; $(-\chi_{dH})$ is the suggested diamagnetic contribution due to the presence of the hydrogen (H) phase captured inside the deep dislocation cores (d). In a high magnetic field ($H > 5$ Oe), this diamagnetic contribution disappears, and the result of the subtraction of χ_{bgr} from χ_{fg} can be written as

$$\Delta\chi_{fg-bgr} = \chi[PdH_x\text{–}Pd] = -\chi_{St} + \Delta\chi_i, \tag{3}$$

where $\Delta\chi_i$ is the weak low-temperature contribution to susceptibility caused by impurities regrouping in the hydrogen-cycled sample. Equation (3) provides a weak almost temperature- and field-independent diamagnetic response. At a low magnetic field ($H < 5$ Oe) and temperature $T < 30$ K, the result of the $\chi_{fg} - \chi_{bgr}$ subtraction (Eq. (2)) can be represented as

$$\begin{aligned} \Delta\chi_{fg-bgr} &= \chi[PdH_x\text{–}Pd] \\ &= -\chi_{dH}(T, H) - \chi_{St} + \Delta\chi_i. \end{aligned} \tag{4}$$

At $T > 30$ K, the term $[-\chi_{dH}(T, H)]$ disappears and Eqs. (2) and (3) become equivalent. Curves *1* and *2* in (Fig. 9) illustrate this effect in low and high magnetic fields at $T > 50$ K. As can be seen, the behavior and absolute values of $\chi(T)$ in both the low (curve *1*) and the high (curve *2*) magnetic fields look similar above 50 K, and the dramatic difference between these two curves begins to appear only at $T < 50$ K.

The results expected from Eqs. (3) and (4) are also obtained for both the net DC-magnetization $\Delta M(T)$ and the real susceptibility $\Delta\chi'(T)$ in a low magnetic field. (Fig. 2a, curve *3* and Fig. 3c). During $M(T)$ ZFC magnetization and measurement at a low field ($H = 0.5$ Oe), a weak negative value of ΔM_{fg-bgr} at $T > 50$ K is followed by a dramatic drop of ΔM in the range 2–50 K. For the AC measurement at $H = 0$, the real part of the susceptibility difference $\Delta\chi'_{fg-bgr}$, shows a similar behavior to that of the DC $M(T)$ experiment at $H = 0.5$ Oe (Fig. 3c). In contrast, a slightly negative, mostly temperature-independent value of ΔM_{fg-bgr} over the whole temperature range 2–298 K is observed in FC measurement at $H = 1000$ Oe (Fig. 2b). Thus, the effect of a drastic ΔM_{fg-bgr} reduction over the temperature range 2–30 K does not emerge in high magnetic fields.

The $M(H)$ and $M(T)$ data for PdH_x(fg), Pd(bgr), and for the net contribution of the PdH_x–Pd phase allow us to suggest that the anomalous diamagnetic response at

temperatures below 30 K in the low magnetic field was induced by the appearance of superconductivity in the Pd hydride phase inside the deep dislocation cores. This suggestion would satisfactorily explain the temperature and field dependences of the PdH_x–Pd net magnetization curves (Figs. 2–7). We note that the net hysteresis loops at $T = 2$ and 10 K are similar to the $M(H)$ characteristics of a nonlinear, irreversible magnetization function of a type II superconductor (Figs. 5b and 7b).

Assuming that the negative value of the initial magnetization taken for the PdH_x–Pd phase at $T = 2$ and 10 K (Figs. 5b and 7b) is evidence of the Meissner effect [36], the local minimum would correspond to a lower critical field $H_{c1} = 3.5 \pm 0.5$ Oe of a type II superconductor. The trace of the local minimum field ascribed to the net PdH_x–Pd phase at $T = 2$ and 10 K also appears as a point of inflection on the virgin (magnetization) part of the $M(H)$ function for the PdH_x(fg) sample (Figs. 5a and 7a, curves *2*). We note that the assumption regarding the type II superconductivity in the PdH_x–Pd phase does not contradict the net low field DC $\Delta M(T)$ and AC $\Delta\chi'(T)$ results at $T < 30$ K (Figs. 2a and 3).

Further indirect evidence of superconductivity below 30 K may be found in the net $\Delta M_r(T)$ remanent magnetization behavior (see inset in Fig. 4). At temperatures greater than 30 K, the $\Delta M_r(T)$ curve has a slightly negative value close to that of $\Delta M(T)$ above $T = 30$ K (Fig. 2a, curve *3*). This negative value of the net remanent magnetization shows that Stoner's contribution at $T > 30$ K plays a major role in the $M(T)$ behavior of the PdH_x–Pd phase even at a very low field. But below 30 K, the net remanent magnetization emerges. The magnitude of $\Delta M_r(T)$ is found to be proportional to the magnitude of the diamagnetic response of the PdH_x–Pd phase at low field (Fig. 9, curve *1*). Such behavior is also expected for a type II superconductor, as seen in the cuprates [37].

The absence of a direct evidence for the diamagnetic effects that characterizes type II superconductors in the PdH_x(fg) sample (e.g., without subtraction of the Pd matrix signal) could possibly be referenced to a very small contribution of diamagnetic response from the hydride phase inside deep dislocation cores to the entire PdH_x paramagnetism. Similar magnetic behavior of a tiny superconducting fraction of $\alpha \approx 5 \times 10^{-4}$ at $T = 1.9$ K ($T_c \approx 3.6$ K) of the Pd nanoparticles sandwiched between graphene sheets (Pd–MG) was recently demonstrated by Suzuki et al. [36].

Indeed, according to our TDA data, the total number of hydrogen atoms involved in hydride formation inside deep dislocation cores should correspond to the value $x = H/Pd \approx 0.04\%$. Assuming that closed dislocation loops are required to observe the diamagnetic signal, the actual fraction of the flux expulsion relative to the complete diamagnetism must be even less than that contributed by the hydrogen content. In this case, only the subtraction of the initial massive Pd matrix from PdH_x magnetization would make it possible to display the superconducting effects in the PdH_x–Pd phase of interest. The other obstacle that could cover a direct diamagnetic response in PdH_x pertains to the paramagnetic Meissner effect and may appear due to the submicron size grain structure (consisting of dislocation subgrains) of the PdH_x crystal after the hydrogen cycling. Such inhomogeneities can be caused by magnetic flux capture on the grain boundaries resulting in a paramagnetic response below T_c at low-field FC [38, 39] and even ZFC [40] measurements.

Assuming that the weak superconductivity actually exists in the PdH_x sample, the penetration depth would be defined as

$$\lambda = \sqrt{\Phi_0/2\pi H_{c1}} = 9.7 \times 10^{-5} \text{ cm},$$

where $\Phi_0 = 2.078 \times 10^{-7}$ G cm is the fluxoid and $H_{c1} = 3.5$ Oe is the lower critical field, taken from Fig. 5b. If the superconducting phase PdH_x–Pd is confined into dislocation subgrains with a radius of $R_s = 60$ nm, then $R_s \ll \lambda$ and we are dealing with the zero-dimension limit of superconductivity [41]. The fluctuation of the diamagnetism above T_c can than be described by the expression

$$\begin{aligned}\chi \text{ [emu/g]} &= -\frac{1}{40\pi}\frac{R_s^2}{\lambda^2}(t-1)^{-1} \\ &= -2.41 \times 10^{-6}(t-1)^{-1},\end{aligned} \quad (5)$$

where $t = T/T_c$. Well below T_c, where fluctuation effects are swamped by the mean-field superconductivity, the magnetic susceptibility should rise as $1 - t$ [41, 42].

These two conditions of the susceptibility behavior above and below T_c allow us to estimate the transition temperature T_c in the PdH_x–Pd zero-dimension system by fitting the $\Delta M(T)$ experimental data (Fig. 2a, curve *3*) with Eq. (5). As seen from Fig. 11, the best full fit of $\Delta M(T)$ above and below T_c can be obtained on the assumption $T_c = 18.0 \pm 1.5$ K. At the same time, the lower T_c fits, including $T_c = 10$ K, cannot satisfactorily describe the $\Delta M(T)$ experimental dependence. We note that $T_c = 18$ K, which reflects a best fit of the net DC moment versus T, is in good agreement with the temperature where the net AC $\Delta\chi'(T)$ dependence begins dropping dramatically (Fig. 3c).

Finally, we note that estimated T_c for the PdH_x–Pd phase, making up the contribution of condensed hydrogen precipitated inside deep dislocation cores in a Pd single crystal, is found to be significantly higher than that measured and calculated for the bulk PdH_x hydrides with $x \approx 1.0$ [15, 18, 19, 43, 44]. Earlier, it was shown that the critical temperature of the superconducting transition in PdH_x is strongly affected by the load-

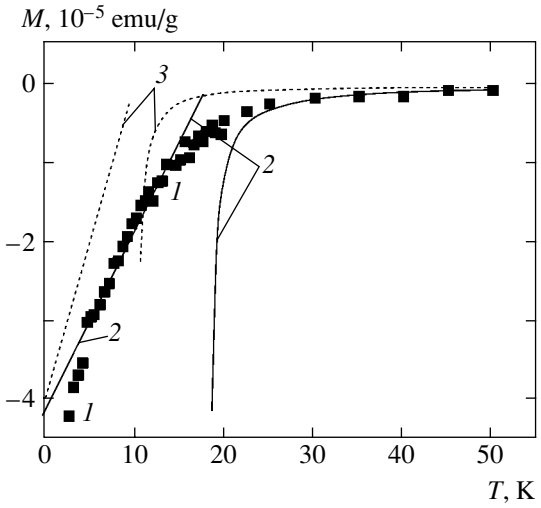

Fig. 11. Fits of the net $\Delta M(T)$ data (curve *1*) taken from Fig. 2a, curve *3* with the diamagnetic susceptibility function (Eq. (5)) above ($\chi \propto (t-1)^{-1}$) and below ($\chi \propto 1-t$) the critical temperature, assuming T_c = 18 (curve *2*) and 10 K (curve *3*).

ing ratio x in the range $0.81 < x \le 1.0$. This observation allows us to estimate roughly the effective value x_{eff} = H/Pd inside deep dislocation cores in a Pd single crystal, assuming T_c = 18 K. Indeed, according to the McMillan equation [45], the expression for T_c in PdH_x-type hydrides at $x > 0.8$ can be written as

$$T_c = \frac{\langle \hbar\omega \rangle}{1.2k_B} \exp\left[-\frac{1.04(1+\lambda_{ep})}{\lambda_{ep} - \mu^*(1+0.62\lambda_{ep})}\right], \qquad (6)$$

where $\langle \hbar\omega \rangle$ is the characteristic average of the phonon energies in the PdH_x phase, including Pd and hydrogen subsystems, λ_{ep} is the electron-phonon coupling constant, $\lambda_{ep} = \lambda_{ep}(Pd) + \lambda_{ep}(H)$, and μ^* is the Coulomb pseudopotential that accounts for repulsive effects between electrons. Equation (6) satisfactorily describes T_c in PdH_x at x = 1.0, $\langle \hbar\omega \rangle$ = 30–45 meV, λ_{ep} = 0.54–0.56, and $\mu^* \approx$ 0.085–0.100, resulting in T_c = 8.0–9.5 K [43]. Substituting well-established parameters $\langle \hbar\omega \rangle$ = 45 meV and $\mu^* \approx 0.10$ from [44, 46] in Eq. (6) versus T_c = 18 K, we obtain λ_{ep} = 0.704. In the case of bulk PdH_1 with λ_{ep} =0.56 and $\lambda_{ep}(Pd)$ = 0.143 [44], we have $\lambda_{ep}(H)$ = 0.417. Similarly, for the PdH_x–Pd phase, we have $\lambda_{ep}(H)$ = 0.561 [18]. Assuming proportionality between the hydrogen concentration x = H/Pd and the magnitude of $\lambda_{ep}(H)$ in highly loaded Pd hydrides ($x > 0.8$), we thus obtain the effective loading ratio inside the deep dislocation core:

$$x_{eff} = 1.0(0.561/0.417) = 1.35.$$

The same magnitude of x = H/Pd could be obtained from a separate consideration, based on a simple equation relating the hydrogen concentration inside dislocations (N_H) to the radius of a segregated hydride cylinder (R_H) inside a dislocation core ([8, Eq. (17)]). Here, we neglect free hydrogen distributed far away from dislocation cores because there is no hydrogen outside deep dislocation cores after annealing at T = 570 K. In such a case, $N_H = \pi x_{eff} N_d R_H^2$ [18]. Using the derived residual concentration $N_H = 4.5 \times 10^{-4}$ and estimated R_H = 2.75 Å, we can obtain x_{eff} = 1.35 if the effective density of dislocations filled with hydrogen is chosen as $N_d = 1.4 \times 10^{11}$ cm^{-2}, corresponding to about 60% of the total estimated number of dislocations after the hydrogen cycling ($N_d \approx 2.5 \times 10^{11}$ cm^{-2}).

In conclusion, the anomalous diamagnetic response from the PdH_x–Pd nanophase observed in this work at temperatures below 30 K in a low magnetic field ($0 < H < 5$ Oe) may indicate the emergence of a weak superconductivity in the Pd matrix. This diamagnetic effect is caused by loading the dislocation cores with a compressed Pd-hydride nanophase. This phase also represents a metastable hydrogen dominant metallic alloy, where both hydrogen and palladium may participate in common overlapping bands due to the large hydrogen binding energy ($\varepsilon_H \approx$ 1.6 eV/atom) inside the deep dislocation cores of a small radius ($R_H \approx$ 2.75 Å). The unique properties of a compressed Pd hydride inside deep dislocation cores make this compound a feasible candidate for the search of HTS in hydrogen dominant metallic alloys [3].

The feasibility of a direct observation of diamagnetic effects in a H_2-cycled PdH_x system could be referenced to reduction of the volume of the paramagnetic Pd relative to that of the dislocation cores filled with a condensed hydrogen phase.

ACKNOWLEDGMENTS

This work was partially supported by the NSF under Grant DMR-9982520. The magnetic measurements were performed at the Center for Microanalysis of Materials at the Frederick Seitz Material Research Laboratory at UIUC. This facility is supported by the U.S. Department of Energy under Grant DEFG02-91-ER45439. The authors thank T. Banks for his help in the arrangement of the magnetic measurements, A. Bezryadin for overall interest in this work and stimulating discussions, and R. Prozorov for his valuable comments on the magnetic measurement results.

REFERENCES

1. Hydrogen Storage "Think Tank" Report, March 14 (Washington, DC, 2003), http://www.eere.energy.gov/hydrogenfuelcels/pdfs/h2_storage_think_tank.html.
2. F. Favier, E. C. Walter, M. P. Zach, et al., Science **293**, 2227 (2001).
3. N. W. Ashcroft, Phys. Rev. Lett. **92**, 187002 (2004).

4. J. Nagamatsu, N. Nakagawa, T. Muranaka, et al., Nature **410**, 63 (2001).
5. B. J. Heuser and J. S. King, Met. Mater. Trans. A **29**, 1594 (1998).
6. W. C. Chen and B. J. Heuser, Phys. Rev. B **65**, 014102 (2002).
7. R. Kirchheim, Acta Metall. **29**, 845 (1981).
8. M. Maxelon, A. Pundt, W. Pyckhout-Hintzen, et al., Acta Mater. **49**, 2625 (2001).
9. R. Kirchheim, Prog. Mater. Sci. **32**, 262 (1988).
10. G. Elsasser, K. M. Ho, C. T. Chan, and M. Fahnle, J. Phys.: Condens. Matter **4**, 5207 (1992).
11. N. W. Ashcroft, Phys. Rev. Lett. **21**, 1748 (1968).
12. T. W. Barbee, A. Garcia, and M. L. Cohen, Nature **340**, 369 (1989).
13. C. F. Richardson and N. W. Ashcroft, Phys. Rev. Lett. **78**, 118 (1997).
14. E. G. Maksimov and D. Yu. Savrasov, Solid State Commun. **119**, 569 (2001).
15. B. Strizker and H. Wuhl, in *Hydrogen in Metals II*, Ed. by G. Alefeld and J. Volkel (Springer, Berlin, 1978), Top. Appl. Phys., Vol. 29, p. 290.
16. L. Schlapbach, I. Anderson, and J. P. Burger, in *Materials Science and Technology*, Ed. by K. H. Jurgen Buschow (Weinheim, New York, 1994), Vol. 3B, Part 2, p. 287.
17. C. Herrero and F. D. Manchester, Phys. Lett. A **86**, 29 (1981).
18. A. G. Lipson, B. J. Heuser, C. H. Castano, and A. Celic, Phys. Lett. A **339**, 414 (2005).
19. A. G. Lipson, B. J. Heuser, C. H. Castano, et al., Phys. Rev. B **72**, 212507 (2005).
20. B. Strizker, Phys. Rev. Lett. **42**, 1769 (1979).
21. J. Miller and C. B. Satterthwaite, Phys. Rev. Lett. **34**, 144 (1975).
22. J. E. Schriber, J. M. Mintz, and W. Wall, Solid State Commun. **52**, 837 (1984).
23. R. Madec, B. Devinere, L. Kubin, et al., Science **301**, 1879 (2003).
24. A. P. Ramirez, K. C. Haddon, O. Zhou, et al., Science **265**, 84 (1994).
25. G. F. J. Garlick and A. F. Gibson, Proc. R. Soc. London, Ser. A **60**, 574 (1948).
26. J. Won, R. P. Doerner, and R. W. Conn, J. Nucl. Mater. **256**, 96 (1998).
27. C. H. Castano, M.S. Thesis (Univ. of Illinois, Urbana, 2002).
28. H. C. Jamieson and F. D. Manchester, J. Phys. F **2**, 323 (1972).
29. D. Mendoza, F. Morales, R. Escudero, and J. Walter, J. Phys: Condens. Matter. **11**, L317 (1999).
30. D. A. Van Leeuwen, J. M. Van Reitebeek, G. Schmidt, and L. J. De Jongh, Phys. Lett. A **170**, 325 (1992).
31. B. Meyer and B. Strizker, Phys. Rev. Lett. **48**, 502 (1982).
32. M. Wilkens, in *Fundamental Aspects of Dislocation Theory*, Ed. by J. A. Simmons, R. de Wit, and R. Bullough (National Bureau of Standards, Washington, 1970; Mir, Moscow, 1977), Vol. 2; NIST Spec. Publ., No. 317 (1969), p. 1195.
33. M. A. Krivoglaz, *X-ray and Neutron Diffraction in Nonideal Crystals* (Springer, Berlin, 1996).
34. D. Breuer and P. Klemanek, J. Appl. Crystallogr. **33**, 1284 (2000).
35. M. Suzuki, I. S. Suzuki, R. Lee, and J. Walter, Phys. Rev. B **66**, 014533 (2002).
36. M. Suzuki, I. S. Suzuki, and J. Walter, J. Phys.: Condens. Matter **16**, 903 (2004).
37. T. Tsebro, O. E. Omelyanovskii, and A. P. Moravski, JETP Lett. **70**, 462 (1999).
38. A. K. Geim, S. V. Dubonos, J. G. S. Lok, et al., Nature **396**, 144 (1998).
39. S. Reidling, G. Bräuchle, R. Lucht, et al., Phys. Rev. B **49**, 13283 (1994).
40. S. Yuan, L. Ren, and F. Li, Phys. Rev. B **69**, 092509 (2004).
41. M. Tinkham, *Introduction to Superconductivity*, 2nd ed. (McGraw-Hill, New York, 1996; Atomizdat, Moscow, 1980).
42. R. A. Buhrman and W. P. Halperin, Phys. Rev. Lett. **30**, 692 (1973).
43. D. A. Papaconstantopoulos, B. M. Klein, E. N. Economou, and L. L. Boyer, Phys. Rev. B **17**, 141 (1978).
44. J. M. Rowe, J. J. Rush, J. E. Schriber, and J. M. Mintz, Phys. Rev. Lett. **57**, 2955 (1986).
45. W. L. McMillan, Phys. Rev. **167**, 331 (1968).
46. J. M. Nicol, J. J. Rush, and R. D. Kelley, Phys. Rev. B **36**, 9315 (1987).